Optical and magnetic control of orbital flat bands in a polariton Lieb lattice

C. E. Whittaker,[1] D. R. Gulevich,[2] D. Biegańska,[1,3] B. Royall,[1] E. Clarke,[4]
M. S. Skolnick,[1,2] I. A. Shelykh,[5,2] and D. N. Krizhanovskii[1,2,*]

[1]*Department of Physics and Astronomy, University of Sheffield, Sheffield S3 7RH, United Kingdom*
[2]*School of Physics and Engineering, ITMO University, St. Petersburg 197101, Russia*
[3]*Department of Experimental Physics, Wrocław University of Science and Technology, Wybrzeże Wyspiańskiego 27, 50-370 Wrocław, Poland*
[4]*EPSRC National Epitaxy Facility, University of Sheffield, Sheffield S1 4DE, United Kingdom*
[5]*Science Institute, University of Iceland, Dunhagi 3, 107 Reykjavik, Iceland*

(Received 14 July 2021; revised 8 October 2021; accepted 23 November 2021; published 9 December 2021)

We study the magneto-optical response of exciton polaritons in *p*-orbital flat bands in a two-dimensional Lieb lattice of semiconductor microcavity pillars. At low excitation density, we detail the influence of an external magnetic field on the exciton component, which enables magnetic tuning of the flat-band states. In the high-density regime, one can induce a spin population imbalance by circularly polarized pumping leading to an effective nonlinear Zeeman splitting. We show how the interplay between the symmetry of the orbital wave function, photonic spin-orbit coupling, and real and effective Zeeman splittings gives rise to real-space flat-band patterns with tilted orbital wave functions in the regime of dynamical polariton condensation. These results demonstrate the ability to optically and magnetically manipulate the spatial, spectral, and polarization properties of polariton condensates in the flat energy bands of a Lieb lattice.

DOI: 10.1103/PhysRevA.104.063505

I. INTRODUCTION

It has been over three decades since the idea of flat energy bands in lattices with certain geometries first sparked theoretical interest [1,2]. Due to the vanishing group velocity in a spectrally flat (dispersionless) band, particle transport is suppressed, leading to increased sensitivity to perturbations and rich phase diagrams of strongly correlated ferromagnetic and topological states [3–5]. It has also long been conjectured that flat bands play a key role in high-temperature superconductivity, the mechanism of which is still not fully understood [6–8]. Currently, there is a strong resurgence of interest in these areas of physics due to recent experimental progress in the development of novel quantum materials featuring flat bands. These include twisted multilayers of graphene [9–13] and dichalcogenides [14,15] exhibiting correlated insulating, superconducting, and ferromagnetic states.

Alongside these advances, the past decade has also seen the emergence of artificial lattices featuring flat bands as a means of studying the associated physics in precisely controlled analog environments [16,17]. In particular, the Lieb lattice [2] has garnered considerable attention and has been implemented in diverse systems including cold atoms [18,19], waveguide arrays [20–22], and engineered atomic lattices [23,24]. While each platform has its own merits, one can combine the appealing aspects of photonic lattices (direct access to the dispersion, wave functions, and coherence properties) with a pronounced nonlinearity and sensitivity to magnetic fields by using semiconductor microcavities hosting exciton polaritons. Exploiting such features along with the driven-dissipative nature of the system, recent studies of flat bands in one-dimensional and two-dimensional (2D) Lieb lattice geometries have elucidated interesting effects including disorder-induced localization [25], nonlinear domain formation [26], and also pseudospin (polarization) patterns [27]. Interestingly, the latter work also studied *p*-type flat bands (previously demonstrated in honeycomb lattices [28]) revealing a distinctive real-space pattern which has since been studied in other platforms [29,30]. This additional degree of freedom highlights the potential of higher-energy flat bands to address questions relating to orbital physics in frustrated media [31].

Further rich insight into the nature of flat bands may be provided by exploring the response to applied magnetic fields, in the spirit of earlier theoretical studies [32] and recent experimental work on kagome magnets [33]. In the case of conventional planar semiconductor microcavities, rich magneto-optical effects have been uncovered over the past two decades including a nontrivial interplay between the Zeeman effect and spin-dependent interactions [34–38] and also a purely optically induced Zeeman effect created by spin-imbalanced pumping [39,40]. In samples which are patterned to introduce a lattice potential, a magnetic or optical Zeeman splitting (ZS) can be used to open topological gaps in graphene and kagome lattices [41,42]. However, in the case of Lieb lattices, magneto-optical effects have not been considered in relation to the polariton flat-band energy spectrum and the spatial and pseudospin properties of the characteristic localized states.

*d.krizhanovskii@sheffield.ac.uk

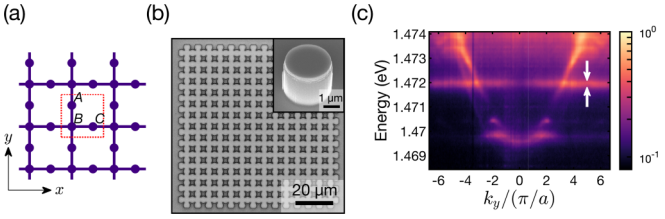

FIG. 1. (a) Geometric structure of the Lieb lattice with three sites (A, B, and C) per unit cell (dotted square). (b) Scanning electron microscope image of the Lieb lattice of overlapping micropillars. The inset shows a single micropillar. (c) Angle-resolved photoluminescence spectrum at $k_x = 0$.

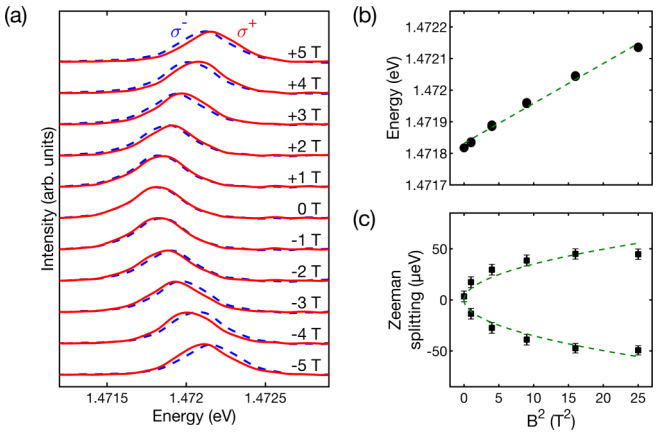

FIG. 2. (a) Magnetic-field dependence of the p flat-band spectrum, from which the (b) diamagnetic shift and (c) Zeeman splitting are extracted. A baseline has been subtracted from the spectra shown in (a). The laser excitation beam is linearly polarized and the excitation power is approximately 500 μW well below the condensation threshold.

In this work we study the influence of real and effective (optically induced) magnetic fields on polaritons in the p flat band (PFB) of a 2D Lieb lattice and demonstrate the ability to affect the spatial, spectral, and polarization properties of the associated emission. In the linear regime, an applied magnetic field induces a diamagnetic shift, ZS, and increase of oscillator strength for the quantum well (QW) exciton, offering a means to tune the polaritonic PFB states. Under higher power excitation we show that the ZS can be controlled via the combined effect of the applied field and the spin population imbalance created under circularly polarized pumping. We also find that circularly polarized pumping modifies the real-space distribution of the cross-polarized spin component of the macroscopically occupied PFB, leading to a broken-symmetry state with tilted orbital wave functions. Our experimental observations are supported by numerical modeling and a phenomenological interpretation.

II. SAMPLE AND EXPERIMENTAL DETAILS

Our sample, which is the same as that of Ref. [27], is a GaAs microcavity featuring three $In_{0.04}Ga_{0.96}As$ QWs and 23 (27) $GaAs/Al_{0.85}Ga_{0.15}As$ top (bottom) distributed Bragg reflector pairs. We etched the top mirror using electron beam lithography and plasma dry etching to define arrays of overlapping micropillars (3 μm diameter and 2.9 μm separation) in a 2D Lieb lattice geometry [see Fig. 1(b)]. The partial etching is sufficient to create a strong confinement potential for photons (and hence polaritons) leading to a gapped band structure. In Fig. 1(c) we see an example of an angle-resolved photoluminescence (PL) spectrum measured at low excitation power below the threshold for polariton condensation [27] showing s- and p-type states (formed from coupling between fundamental and first excited modes of the micropillars, respectively) which both feature flat bands. We focus on the p flat band (marked by white arrows) in this work due to its larger exciton fraction, which facilitates both optical and magnetic control.

In order to study magneto-optical effects the sample is mounted in a superconducting magnet cryostat and fields up to $B = \pm 5$ T are applied in the Faraday configuration. The sample is addressed in the reflection geometry. Polarization optics are used in the collection path (quarter waveplate and linear polarizer) in order to spectrally resolve the ZS of polariton states and also in the excitation path (quarter waveplate) to control the polarization state of the excitation laser. To perform measurements of PL power dependences we use continuous-wave excitation with the laser tuned to approximately 2 meV above the exciton energy (at 0 T) such that it is always resonant with upper polariton or excitonic states. In contrast to excitation high above the band gap, such conditions create a cool exciton distribution, preventing creation of excess hot carriers which lead to a collapse of strong coupling before high polariton densities can be reached [43]. We use a spot size of approximately 15 μm and excitation angles of approximately 10°–15° (in the direction orthogonal to the spectrometer slit) to avoid a large reflected laser signal in angle-resolved spectra.

III. EXPERIMENTAL RESULTS

First we will consider low-power (far below threshold of condensation into the flat band) excitation. In this low-density regime, the energy $E^{\pm}_{\mathrm{PFB}}$ of the polariton PFB (where $\pm$ denotes the spin state) can be modified via the QW exciton component by applying a magnetic field. Under a finite field, the average exciton energy $E_X = (E^+_X + E^-_X)/2$ is blueshifted by $\delta E^{\mathrm{dia}}_X = \kappa_X B^2$, where κ_X is the effective diamagnetic factor of the exciton. Also, there is a ZS between the two exciton spin components given by $\Delta E^{\pm,Z}_X = \pm\frac{1}{2} g_X \mu_B B$, where g_X is the effective g factor of the exciton and μ_B is the Bohr magneton. Finally, there is an enhancement of the Rabi splitting Ω due to the increase of exciton oscillator strength f, given by $\Omega(B) = \Omega(0)\sqrt{f(B)/f(0)}$ [44]. To estimate the energy change of the *polariton* mode $E^{\pm}_{\mathrm{PFB}}$, one can account for the diamagnetic shift and Zeeman splitting of the exciton energy, weighted by the exciton fraction $|X|^2(B) = (1 + \Delta/\sqrt{\Delta^2 + \Omega^2})/2$, where Δ is the cavity-exciton detuning.

In our sample, $\Omega \approx 4.7$ meV and the PFB has $|X|^2 \sim 18\%$. In order to demonstrate magnetic tuning of the PFB we perform a magnetic-field dependence going from -5 to $+5$ T (Fig. 2). We observe blueshifts of approximately 0.3 meV at ± 5 T and a ZS of approximately 50 μeV. These are both larger than expected if only taking into account $\delta E^{\mathrm{dia}}_X$ and

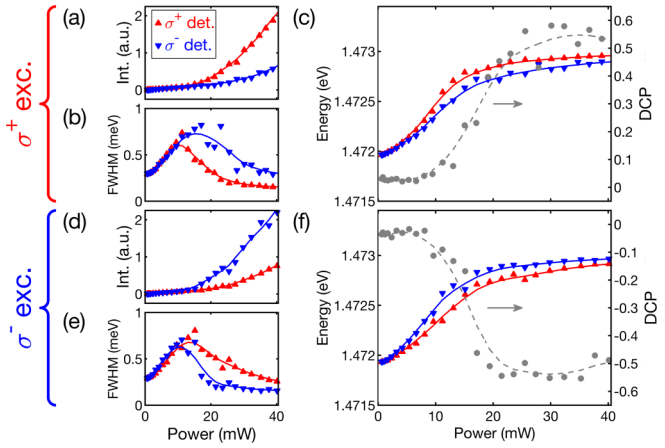

FIG. 3. (a) Intensity, (b) full width at half maximum, and (c) energy of the p flat band measured under σ^+ excitation. The right axis in (c) shows the degree of circular polarization of the emission. (d)–(f) Same as (c)–(e) but for σ^- excitation. For these measurements $B = 0$ T. Solid and dashed lines are a guide to the eye.

$\Delta E_X^{\pm,Z}$. However, from planar region measurements, we estimate that the value of Ω increases by approximately 1 meV at ± 5 T compared to 0 T, which serves to counteract the diminishing $|X|^2(B)$ caused by the decrease of Δ at finite fields. Although the true analytical dependence of $E_{\mathrm{PFB}}^{\pm}$ on B [which would take into account the dependence of $\Omega(B)$ and $|X|^2(B)$ as well] is not known, as a coarse approximation the effective diamagnetic factor $\kappa_{\mathrm{PFB}} \sim 13\ \mu\mathrm{eV/T}^2$ and the g factor $g_{\mathrm{PFB}} \sim 0.2$, as shown by green dashed lines in Fig. 2 (cf. $\kappa_X \sim 85\ \mu\mathrm{eV/T}^2$ and $g_X \sim 1.25$ for the bare exciton). Now we consider increasing the excitation power, first in the absence of an applied field. Altering the total population $n = n^+ + n^-$ of polaritons and excitons (excitonlike polaritons with high momenta or so-called exciton reservoir) in the system allows $E_{\mathrm{PFB}}^{\pm}$ to be modified, again via the exciton component. In bare QWs, as the number of excitons increases there is a complex self-energy term accounting for the blueshift (real part) and broadening (imaginary part) induced by mutual Coulomb interactions [45]. The interactions are spin dependent, as revealed under $\sigma^{\pm}$ (circularly polarized) excitation where an energy splitting appears between excitons copolarized and cross polarized with the pump. In strongly coupled microcavities the polariton blueshift is given by $\Delta E^{\pm} = \alpha_1 n^{\pm} + \alpha_2 n^{\mp}$, where α_1 and α_2 are detuning-dependent interaction constants for polaritons with the same and opposite spins, respectively [46], with $\alpha_1 \gg \alpha_2$. Interaction-induced circular polarization splittings constitute an effective ZS which can be controlled optically using the excitation polarization. To demonstrate the influence of this behavior on $E_{\mathrm{PFB}}^{\pm}$ we perform power dependences under $\sigma^{\pm}$ excitation and measure the co- and cross-polarized emission intensity of the PFB, which is summarized in Fig. 3.

The circularly polarized pump creates the population of high-density exciton reservoir and high-energy polaritons, which is predominantly copolarized with the pump. However, at the lowest powers, the slow population of lower polariton states dominated by acoustic phonon scattering leads to almost total spin relaxation such that the degree of circular polarization (DCP) of the emission and the ZS remain zero. The polariton spin relaxation may occur via TE-TM splitting and other splittings of the microcavity photonic mode [40]. High-energy excitons (excitonlike polaritons) are likely to lose their spin via the combination of exchange electron-hole interactions and spin-orbit coupling acting on electrons and holes. As the power is increased, the scattering between polaritons and excitons leads to enhanced relaxation to the lower polariton states [47–49]. Since there is an initial imbalance between populations of circularly polarized excitons and polaritons n^+ and n^- induced by the circularly polarized pump, the copolarized polariton population relaxes faster to the lower-energy states [50]. This leads to the intensity of the copolarized emission from the flat-band states overtaking the cross-polarized component and giving rise to a nonzero DCP and ZS. In this case the polariton blueshift arises from (i) the interactions between polaritons within the flat band itself and (ii) the interactions between the flat-band polaritons and higher-energy excitons and polaritons. The ZS is therefore proportional to the total population imbalance in this regime. We note that at intermediate powers (less than 10 mW) this imbalance already leads to observable ZS of approximately 50–100 μeV for $E_{\mathrm{PFB}}^{\pm}$, whereas the dependence of emission intensity $I^{\pm}$ in this regime is identical for the two spin components (DCP is nearly zero), indicating still a complete polariton depolarization during relaxation. At a power of around 13 mW, the threshold for stimulated scattering into the PFB and subsequent condensation is reached [27] for the copolarized component, as evidenced by a superlinear increase in its emission intensity and pronounced linewidth narrowing by a factor of approximately 2 [Figs. 3(a) and 3(b)]. There is also a sharp increase in the DCP to values of approximately 60% and the ZS reaches peak values of approximately 0.2 meV, which is several times larger than that measured in the linear regime under a real field of ± 5 T. A further increase of the power switches on the interactions between excitons and polaritons with the polarization opposite to that of the pump leading to a threshold for the cross-polarized component which reduces the ZS. We note that at high powers macroscopic occupation of gap states (formed from the top of the s-type antibonding band) and the s flat band also occurs as was previously observed [27], although in this work we focus solely on the PFB.

We also performed power dependences at $B = \pm 5$ T in order to study the interplay between the real and optically induced ZS. The dependences of the ZS on the excitation power for σ^+ and σ^- circularly polarized excitation and for different values of magnetic field are shown in Fig. 4. We note that the excitation conditions are not exactly the same owing to the exciton diamagnetic shift, meaning the pump state population and relaxation dynamics are affected. Nevertheless, we observe in addition to the real ZS an optically induced contribution of more or less the same size, which is maximized at the threshold powers of approximately 15–20 mW. Since the latter exceeds the former, it can be used to counteract or enhance the splitting. In the case of linearly polarized excitation, the real ZS survives above threshold, confirming strong coupling. In all cases, as seen from Fig. 4, above-threshold ZS gradually reduces with power, since it is possibly screened by the interactions, phase synchronization

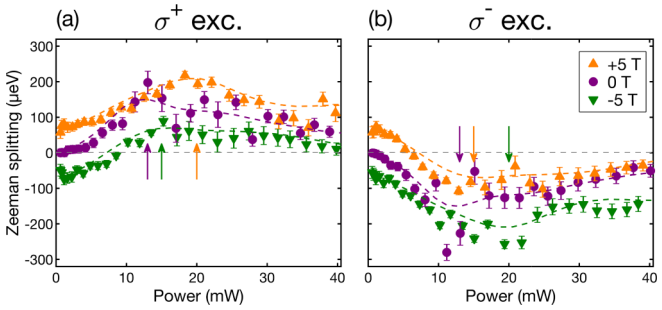

FIG. 4. Power dependence of the p flat-band Zeeman splitting for different magnetic-field strengths under (a) σ^+ and (b) σ^- excitation. The arrows show the onset of stimulated scattering. The dashed lines are a guide to the eye.

between cross-polarized condensates, and thermalization at increasing powers, as has previously been reported in other works [35,36]. The role of exciton reservoir on the ZS in the high-power regime is not fully understood. Viña *et al.* [51] showed that the depolarization rate of excitons in GaAs quantum wells decreases at high exciton density, thus increasing the polarization degree of the reservoir. If this were the case, we would expect that the interactions with the reservoir should increase rather than decrease ZS with excitation power. However, this effect may depend on particular sample characteristics (doping levels, QW thickness, and barrier composition).

These findings show the possibility of spectral tuning of the PFB using the external parameters of magnetic-field strength and excitation power or polarization. Now we discuss the pseudospin properties of the emission, which are also affected. The normal-to-plane component of pseudospin is given by the normalized Stokes component of PFB emission $S_3 = (I^+ - I^-)/(I^+ - I^-)$. In the case of linearly polarized excitation and zero magnetic field, $S_3 = 0$ and the PFB real-space distribution shows pronounced horizontal and vertical polarization on A and C sublattices, respectively, due to linear (TE-TM) polarization splitting. This is the typical pseudospin pattern of the eigenstates of the Lieb lattice PFB in the presence of spin-orbit coupling [27]. When $\sigma^\pm$ excitation is used, the pseudospin acquires an out-of-plane component as evidenced by the large DCP [see Figs. 3(c) and 3(f)] which is given by $\rho = S_3$, and the emission becomes elliptically polarized as a result. We show an example of the above-threshold emission under σ^+ excitation in Fig. 5, where we see the characteristic linear polarization pattern (revealed by the Stokes parameter $S_1 = \frac{I_H - I_V}{I_H - I_V}$, where $I_{H,V}$ is the emission intensity detected in horizontal and vertical polarizations) and optically acquired circular polarization component (revealed by the Stokes parameter S_3). Opposite behavior is observed under σ^- excitation. Interestingly, under an applied field, the ZS induces a nonzero DCP at the lowest powers, which can be made to change sign above threshold under cross-polarized excitation.

We note that the pattern seen in the total emission intensity, given by the Stokes parameter S_0 [Fig. 5(a)], remains the same regardless of excitation polarization or applied field. Namely, emission from the A (C) sites is dominated by the p_x (p_y) orbitals and there is a marked absence of emission

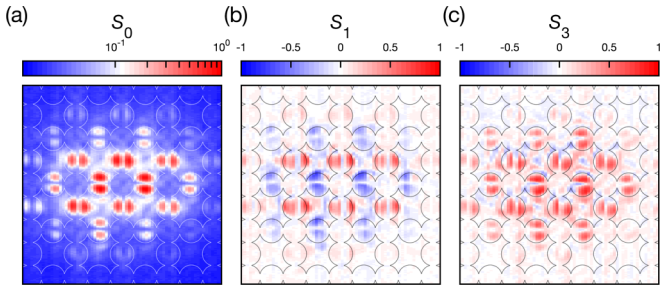

FIG. 5. Measured realspace Stokes parameters (a) S_0, (b) S_1, and (c) S_3 above threshold under σ^+ excitation and no applied field. An outline of the lattice is shown for scale (the pillar diameter is 3 μm)

from B sites. This is a signature of the PFB, arising from the specific lattice geometry and direction-dependent overlap (or tunneling energy) of the p-type pillar modes [27].

However, in our $\sigma^\pm$-resolved images, we observe that the PFB pattern differs between the two spin components (see Fig. 6). Specifically, the orientation of p-orbital lobes is tilted, lowering the C_4 rotational symmetry, in the cross-polarized spin component, i.e., σ^- (σ^+) when exciting with σ^+ (σ^-). As we explain in the following section, the cause of such an effect is the asymmetric population of the PFB in k space, which implies a broken-symmetry state. This asymmetry can be seen in polarization-resolved measurements of the k-space distribution of the PFB above condensation threshold. Interestingly, we find that the same behavior is observed across a broad range of excitation angles and even when the sample is excited at normal incidence.

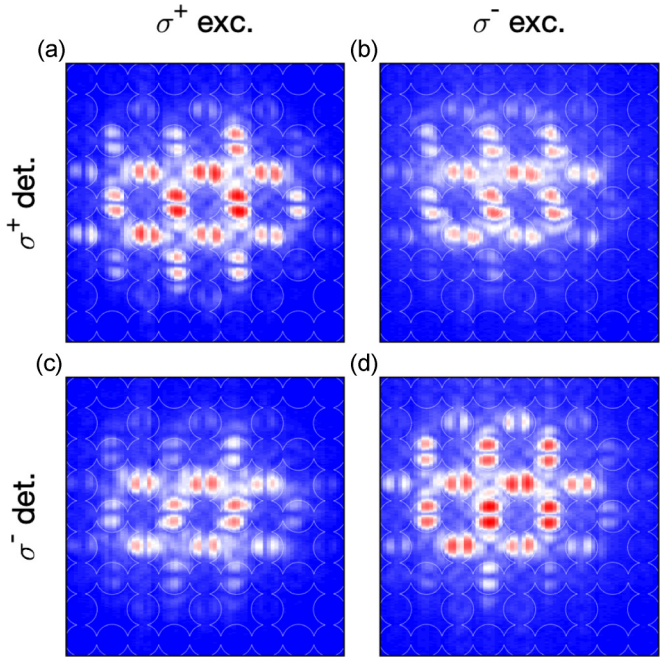

FIG. 6. Measured real-space emission of the PFB resolved in circular polarization. (a) and (d) When the excitation and detection are copolarized, the pattern has C_4 rotational symmetry, whereas (b) and (c) when the excitation and detection are cross polarized, the pattern lacks C_4 rotational symmetry. An outline of the lattice is shown for scale (the pillar diameter is 3 μm).

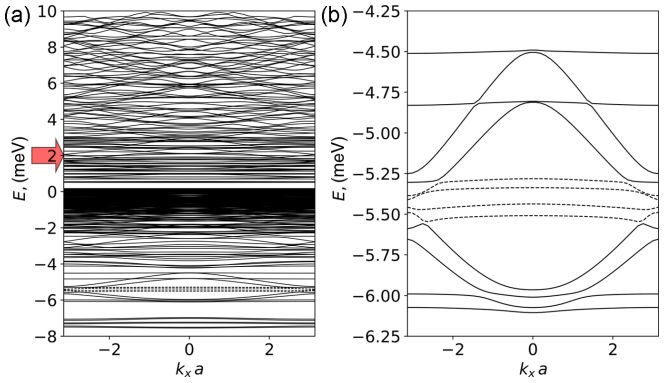

FIG. 7. Band diagram for polaritons in microcavity pillars arranged in the form of a Lieb lattice, calculated using the linear model (1) at $k_y = 0$ and parameters given in the text. The flat bands are highlighted in dashed lines in both panels. The arrow in (a) indicates the coherent pump at energy 2 meV above the exciton level. (b) Close-up of the p flat-band region of interest where the condensation occurs. The four p flat-band dispersions are nondegenerate due to the presence of the finite effective Zeeman and TE-TM splittings.

IV. THEORY

To understand the main qualitative features observed in the experiment, we start with the analysis of the structure of the eigenstates, corresponding to the p flat bands of polaritonic Lieb lattice. We use the Hamiltonian

$$H = \begin{pmatrix} \delta_{\rm det} - \frac{\nabla^2}{2m^*} + U & \beta(\partial_x - i\partial_y)^2 & \frac{\Omega_R}{2} & 0 \\ \beta(\partial_x + i\partial_y)^2 & \delta_{\rm det} - \frac{\nabla^2}{2m^*} + U & 0 & \frac{\Omega_R}{2} \\ \frac{\Omega_R}{2} & 0 & \Omega & 0 \\ 0 & \frac{\Omega_R}{2} & 0 & -\Omega \end{pmatrix} \quad (1)$$

written in the basis $\{\psi_+, \psi_-, \chi_+, \chi_-\}$, where $\psi_\pm$ and $\chi_\pm$ are photon and exciton degrees of freedom, respectively. Here $\delta_{det} = -8$ meV is the exciton-photon detuning, $m^* = 5 \times 10^{-5} m_e$ is the effective mass, $\beta = 0.1$ meV μm^2 is the parameter responsible for the TE-TM splitting, and $\Omega_R = 4.7$ meV is the Rabi frequency. The phenomenological parameter $\Omega = -0.25$ meV is introduced to capture the Zeeman shift of the exciton components (note that the corresponding values for the Zeeman splitting of the polariton components are reduced by the Hopfield coefficient). The photon potential is modeled by taking in the form of the Lieb lattice formed by round pillars of 1.5 μm in diameter. The $U(x, y)$ is zero inside a pillar and takes the value 8 meV outside. This model was used to reproduce the flat bands observed previously in Ref. [27].

The arising band structure is shown in Fig. 7. At energies above -4 meV (with respect to the exciton level) a quasicontinuum of polariton modes is formed and the arrow illustrates schematically the coherent pump at 2 meV above the exciton level into the continuum upper polariton modes as in the experiment. Figure 7(b) shows the zoom of the p flat-band region with the flat bands of interest where the condensation occurs shown in yellow. The presence of the TE-TM splitting and the interaction-induced Zeeman splitting [controlled by Ω in the model (1)] lifts the degeneracy of p flat band into four separated branches. The two lowest-energy flat bands are predominantly σ^--circularly polarized and the other two flat bands are σ^+-circularly polarized. In the experiment, we only observe Zeeman splitting between the cross-polarized emission from the p flat bands. The splitting in the same circular polarization is not observed due to finite linewidth of polariton emission (approximately equal to 100 μeV). The structure of the spin-resolved components of the eigenstates is shown in Fig. 8. At $k_x = k_y = 0$ the eigenstates are symmetric with respect to fourfold rotation [Figs. 8(a) and 8(b)], whereas away from the Brillouin zone center, the presence of a nonzero $k_x = k_y = 0.2\pi/a$ breaks the C_4 rotational symmetry and leads to appearance of a tilted pattern [Figs. 8(c) and 8(d)]. Notice that tilting appears in the weaker component, whereas the tilting of the stronger component remains marginal, as is the case in experiment. The tilting pattern depends on the effective Zeeman splitting which is demonstrated in Figs. 8(e) and 8(f), calculated at larger values of the Zeeman splitting. Figures 8(g) and 8(h) illustrate how the symmetry of the pattern is changed if k_y changes the sign. In the experiment, we record the real-space images by collecting the emission from all k vectors of the p flat band. Thus, the tilting of the p-orbital lobes will appear in real space if the momentum space distribution of polariton condensate emission is asymmetric with respect to x or y axis cutting through $k = 0$, which could form in the nonequilibrium condensates by the relaxation processes [52,53].

Relaxation from the pump to the p flat bands in the condensation regime mainly occurs via polariton-polariton and polariton-excitons scattering since scattering with phonons is not efficient [47]. Thus, to model the condensation into the p flat bands and reproduce the experimentally observed tilting in Fig. 6, we have carried out a numerical simulation of the dynamics of the coupled exciton-photon system in the regime of coherent optical driving where relaxation takes place via coherent scattering [48]. We use the system of coupled nonlinear equations

$$\begin{aligned} i\frac{\partial\psi_+}{\partial t} &= \delta_{\rm det}\psi_+ - \frac{\nabla^2}{2m^*}\psi_+ + U(x,y)\psi_+ - \frac{i}{2}\gamma(x,y)\psi_+ + \beta(\partial_x - i\partial_y)^2\psi_- + \frac{\Omega_R}{2}\chi_+ + P(x,y)A_+e^{i\mathbf{Kr}-i\omega t}, \\ i\frac{\partial\psi_-}{\partial t} &= \delta_{\rm det}\psi_- - \frac{\nabla^2}{2m^*}\psi_- + U(x,y)\psi_- - \frac{i}{2}\gamma(x,y)\psi_- + \beta(\partial_x + i\partial_y)^2\psi_+ + \frac{\Omega_R}{2}\chi_- + P(x,y)A_-e^{i\mathbf{Kr}-i\omega t}, \\ i\frac{\partial\chi_+}{\partial t} &= \frac{\Omega_R}{2}\psi_+ + \left(-\frac{i}{2}\Gamma_X + |\chi_+|^2 + \alpha|\chi_-|^2\right)\chi_+, \quad i\frac{\partial\chi_-}{\partial t} = \frac{\Omega_R}{2}\psi_- + \left(-\frac{i}{2}\Gamma_X + |\chi_-|^2 + \alpha|\chi_+|^2\right)\chi_-, \end{aligned} \quad (2)$$

where $\alpha = -0.05$ is the interaction parameter for opposite polarizations, the exciton damping parameter $\Gamma_X = 1$ meV, and the photon damping $\gamma(x, y)$ takes values of 0.1 meV in the pillar center and 0.5 meV outside the pillar. We

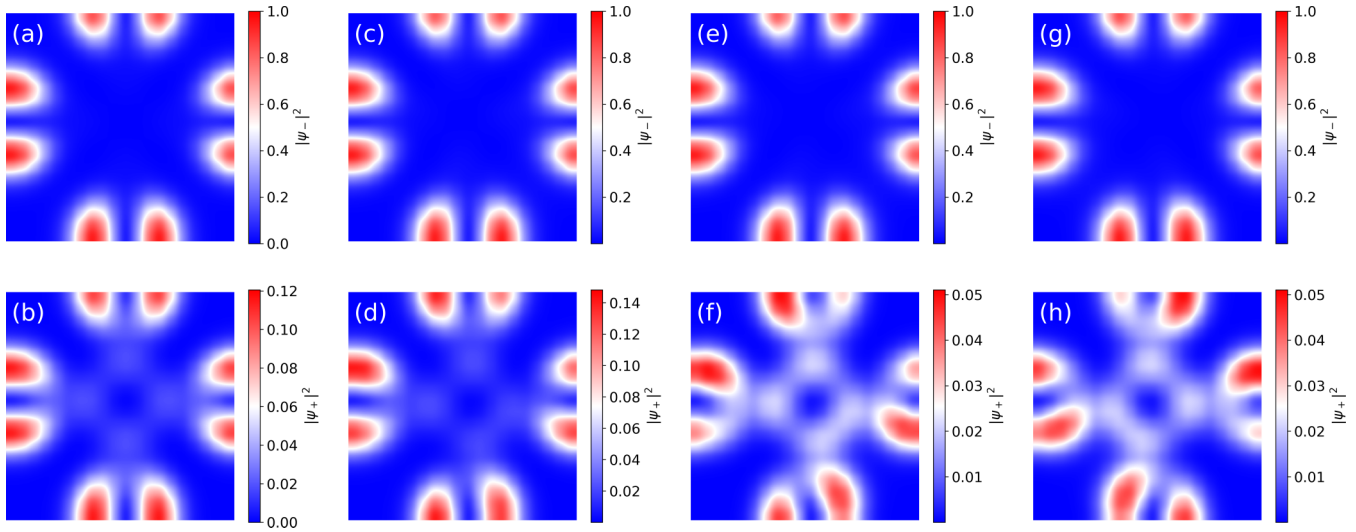

FIG. 8. Real-space profile of the polariton density (its photon component is shown) in a single unit cell of the Lieb lattice (in the experiment the size of the unit cell is 5.8 μm) for the second lowest p flat-band eigenmode responsible for the observed tilting effect, corresponding to (a) and (b) $k_x = k_y = 0$ and $\Omega = -0.25$ meV and (c) and (d) $k_x = k_y = 0.2\pi/a$ and the same value of Ω. Notice that tilting appears in the weaker component, whereas the tilting of the stronger component remains marginal. The tilting pattern depends on the effective Zeeman splitting which is demonstrated in (e)–(h), calculated at twice larger Zeeman splitting, $\Omega = -0.5$ meV, and (e) and (f) $k_x = k_y = 0.2\pi/a$ and (g) and (h) $k_x = -k_y = 0.2\pi/a$. Note the changes in the pattern symmetry [in (d) and (h)] as k_y changes the sign.

simulate a coherent excitation at the pump frequency $\omega =$ 2 meV covering few lattice cells. We model the asymmetric occupation of the flat band observed in the experiments by taking an oblique incidence of the pump beam. The results of our simulation for driving by the primary σ^+ polarization (with a 30% mix of the weaker component to mimic a slight ellipticity which is likely present in the experiments) with nonzero $\mathbf{K}$ are shown in Fig. 9. When the sufficient pump intensity is reached, the p flat band gets populated by the nonlinear coherent scattering. In qualitative agreement with our experimental observations in Fig. 6 and considerations based on the linear model above, the dominant (copolarized with the pump) component is minimally perturbed, remaining largely unaffected by the asymmetric k-space distribution, whereas the weaker component appears to be strongly tilted.

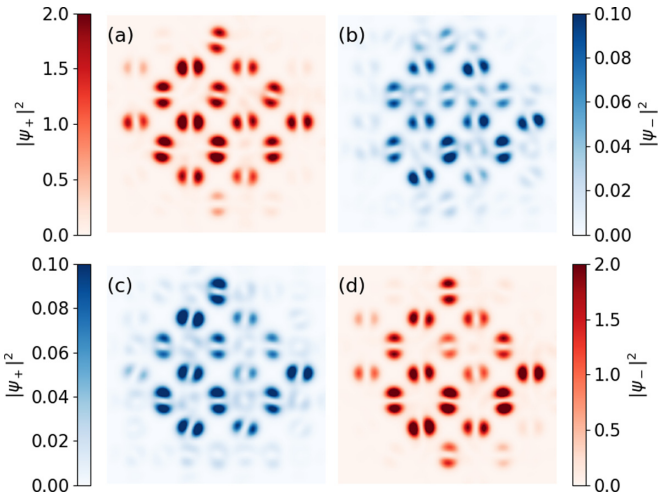

FIG. 9. Patterns observed in the results of our numerical modeling of p flat-band excitation by a resonant pumping with a primary (a) and (b) σ^+ and (c) and (d) σ^- polarization. A 30% mixture of the weaker component is also present in the pump model to account for some degree of ellipticity of the pump [σ^- in (a) and (b) and σ^+ in (c) and (d)]. The patterns observed in the dominating components are shown in (a) and (d). Each panel shows the real-space area 4×4 unit cells of the Lieb lattice.

A change in the orientation of the pump $K_y \to -K_y$ results in a rotation of the tilted pattern by 90°. This confirms that in our numerical model the pump k vector is explicitly responsible for the observed tilting, since it induces an asymmetric occupation of the Brillouin zone of the p flat-band states. However, in the experiment, no change of tilting orientation was observed with the change of the excitation k vector. This implies there are other factors which lead to an asymmetric population in k space and thus to the observed tilting of p flat-band patterns, such as spatial asymmetry of the excitation spot and the presence of slight birefringence in individual pillars. The asymmetry may also arise from complex spatiotemporal dynamics governed by the pump, decay, spinor interactions, and spin-orbit coupling [54,55] which are difficult to model and beyond the scope of our work. Further investigations are needed to obtain a better understanding of this mechanism in our driven-dissipative system. We note that the scenario of a spontaneous symmetry breaking should be excluded, as experimentally observed tilting patterns are consistently reappearing under the same conditions in multiple realizations of the experiment.

Note that there is an alternative view of the flat-band states in the Lieb lattice system. While our linear model (1) which we used to demonstrate the tilting effect assumes an infinite extension of the condensate, compact localized states which form in a single unit cell or extend just over a few lattice sites [1] may arise in the Lieb lattice owing to the high degeneracy of the flat-band energy level, as shown in Ref. [56]. While the

experimentally observed states extend over four lattice sites on average, this can be regarded as an intermediate regime between the fully excited Lieb lattice and the compact localized excitation in Ref. [56]. Thus, the compact localized excitation view may in principle give new insight into the origin of the titling, the discussion of which we leave outside the scope of the present work.

V. CONCLUSION

To conclude, we have performed detailed magneto-optical studies of the *p*-type flat band of a two-dimensional Lieb lattice for polaritons in linear and nonlinear regimes. We have demonstrated that the spatial, spectral, and pseudospin properties of the emission can be modified depending on the combination of magnetic-field strength, optical pumping power, and excitation polarization. Such magnetic and optical manipulation of the polariton wave function is of significant contemporary interest in light of topological photonics at optical frequencies, particularly in the absence of applied fields.

ACKNOWLEDGMENTS

The experimental work was supported by UK EPSRC Grants No. EP/N031776/1, No. EP/R04385X/1, and No. EP/V026496/1. Calculations by I.A.S. using the linear model were supported by the Icelandic Research Fund, Grant No. 163082-051. Numerical calculations of the condensate dynamics in the nonlinear regime were supported by the Russian Science Foundation Grant No. 19-72-20120.

[1] B. Sutherland, Phys. Rev. B **34**, 5208 (1986).
[2] E. H. Lieb, Phys. Rev. Lett. **62**, 1201 (1989).
[3] N. Regnault and B. A. Bernevig, Phys. Rev. X **1**, 021014 (2011).
[4] D. N. Sheng, Z.-C. Gu, K. Sun, and L. Sheng, Nat. Commun. **2**, 389 (2011).
[5] A. Dauphin, M. Müller, and M. A. Martin-Delgado, Phys. Rev. A **93**, 043611 (2016).
[6] N. B. Kopnin, T. T. Heikkilä, and G. E. Volovik, Phys. Rev. B **83**, 220503(R) (2011).
[7] S. Peotta and P. Törmä, Nat. Commun. **6**, 8944 (2015).
[8] A. Julku, S. Peotta, T. I. Vanhala, D.-H. Kim, and P. Törmä, Phys. Rev. Lett. **117**, 045303 (2016).
[9] Y. Cao, V. Fatemi, A. Demir, S. Fang, S. L. Tomarken, J. Y. Luo, J. D. Sanchez-Yamagishi, K. Watanabe, T. Taniguchi, E. Kaxiras, R. C. Ashoori, and P. Jarillo-Herrero, Nature (London) **556**, 80 (2018).
[10] Y. Cao, V. Fatemi, S. Fang, K. Watanabe, T. Taniguchi, E. Kaxiras, and P. Jarillo-Herrero, Nature (London) **556**, 43 (2018).
[11] A. L. Sharpe, E. J. Fox, A. W. Barnard, J. Finney, K. Watanabe, T. Taniguchi, M. A. Kastner, and D. Goldhaber-Gordon, Science **365**, 605 (2019).
[12] K.-T. Tsai, X. Zhang, Z. Zhu, Y. Luo, S. Carr, M. Luskin, E. Kaxiras, and K. Wang, Correlated superconducting and insulating states in twisted trilayer graphene moire of moire superlattices, Phys. Rev. Lett. **127**, 166802 (2021).
[13] X. Liu, Z. Hao, E. Khalaf, J. Y. Lee, Y. Ronen, H. Yoo, D. Haei Najafabadi, K. Watanabe, T. Taniguchi, A. Vishwanath, and P. Kim, Nature (London) **583**, 221 (2020).
[14] L. An, X. Cai, D. Pei, M. Huang, Z. Wu, Z. Zhou, J. Lin, Z. Ying, Z. Ye, X. Feng, R. Gao, C. Cacho, M. Watson, Y. Chen, and N. Wang, Nanoscale Horiz. **5**, 1309 (2020).
[15] E. C. Regan, D. Wang, C. Jin, M. I. Bakti Utama, B. Gao, X. Wei, S. Zhao, W. Zhao, Z. Zhang, K. Yumigeta, M. Blei, J. D. Carlström, K. Watanabe, T. Taniguchi, S. Tongay, M. Crommie, A. Zettl, and F. Wang, Nature (London) **579**, 359 (2020).
[16] D. Leykam, A. Andreanov, and S. Flach, Adv. Phys.: X **3**, 1473052 (2018).
[17] D. Leykam and S. Flach, APL Photon. **3**, 070901 (2018).
[18] G.-B. Jo, J. Guzman, C. K. Thomas, P. Hosur, A. Vishwanath, and D. M. Stamper-Kurn, Phys. Rev. Lett. **108**, 045305 (2012).
[19] S. Taie, H. Ozawa, T. Ichinose, T. Nishio, S. Nakajima, and Y. Takahashi, Sci. Adv. **1**, e1500854 (2015).
[20] D. Guzmán-Silva, C. Mejía-Cortés, M. A. Bandres, M. C. Rechtsman, S. Weimann, S. Nolte, M. Segev, A. Szameit, and R. A. Vicencio, New J. Phys. **16**, 063061 (2014).
[21] R. A. Vicencio, C. Cantillano, L. Morales-Inostroza, B. Real, C. Mejía-Cortés, S. Weimann, A. Szameit, and M. I. Molina, Phys. Rev. Lett. **114**, 245503 (2015).
[22] S. Mukherjee, A. Spracklen, D. Choudhury, N. Goldman, P. Öhberg, E. Andersson, and R. R. Thomson, Phys. Rev. Lett. **114**, 245504 (2015).
[23] R. Drost, T. Ojanen, A. Harju, and P. Liljeroth, Nat. Phys. **13**, 668 (2017).
[24] M. R. Slot, T. S. Gardenier, P. H. Jacobse, G. C. P. van Miert, S. N. Kempkes, S. J. M. Zevenhuizen, C. M. Smith, D. Vanmaekelbergh, and I. Swart, Nat. Phys. **13**, 672 (2017).
[25] F. Baboux, L. Ge, T. Jacqmin, M. Biondi, E. Galopin, A. Lemaître, L. Le Gratiet, I. Sagnes, S. Schmidt, H. E. Türeci, A. Amo, and J. Bloch, Phys. Rev. Lett. **116**, 066402 (2016).
[26] V. Goblot, B. Rauer, F. Vicentini, A. Le Boité, E. Galopin, A. Lemaître, L. Le Gratiet, A. Harouri, I. Sagnes, S. Ravets, C. Ciuti, A. Amo, and J. Bloch, Phys. Rev. Lett. **123**, 113901 (2019).
[27] C. E. Whittaker, E. Cancellieri, P. M. Walker, D. R. Gulevich, H. Schomerus, D. Vaitiekus, B. Royall, D. M. Whittaker, E. Clarke, I. V. Iorsh, I. A. Shelykh, M. S. Skolnick, and D. N. Krizhanovskii, Phys. Rev. Lett. **120**, 097401 (2018).
[28] T. Jacqmin, I. Carusotto, I. Sagnes, M. Abbarchi, D. D. Solnyshkov, G. Malpuech, E. Galopin, A. Lemaître, J. Bloch, and A. Amo, Phys. Rev. Lett. **112**, 116402 (2014).
[29] L. Ma, W.-X. Qiu, J.-T. Lü, and J.-H. Gao, Phys. Rev. B **99**, 205403 (2019).
[30] Y. Chen and H. Chen, New J. Phys. **21**, 113046 (2019).
[31] Y. Tokura and N. Nagaosa, Science **288**, 462 (2000).
[32] H. Aoki, M. Ando, and H. Matsumura, Phys. Rev. B **54**, R17296 (1996).
[33] J.-X. Yin, S. S. Zhang, G. Chang, Q. Wang, S. S. Tsirkin, Z. Guguchia, B. Lian, H. Zhou, K. Jiang, I. Belopolski, N. Shumiya, D. Multer, M. Litskevich, T. A. Cochran, H. Lin, Z. Wang, T. Neupert, S. Jia, H. Lei, and M. Z. Hasan, Nat. Phys. **15**, 443 (2019).

[34] Y. G. Rubo, A. V. Kavokin, and I. A. Shelykh, Phys. Lett. A **358**, 227 (2006).
[35] A. V. Larionov, V. D. Kulakovskii, S. Höfling, C. Schneider, L. Worschech, and A. Forchel, Phys. Rev. Lett. **105**, 256401 (2010).
[36] P. Walker, T. C. H. Liew, D. Sarkar, M. Durska, A. P. D. Love, M. S. Skolnick, J. S. Roberts, I. A. Shelykh, A. V. Kavokin, and D. N. Krizhanovskii, Phys. Rev. Lett. **106**, 257401 (2011).
[37] J. Fischer, S. Brodbeck, A. V. Chernenko, I. Lederer, A. Rahimi-Iman, M. Amthor, V. D. Kulakovskii, L. Worschech, M. Kamp, M. Durnev, C. Schneider, A. V. Kavokin, and S. Höfling, Phys. Rev. Lett. **112**, 093902 (2014).
[38] C. Sturm, D. Solnyshkov, O. Krebs, A. Lemaître, I. Sagnes, E. Galopin, A. Amo, G. Malpuech, and J. Bloch, Phys. Rev. B **91**, 155130 (2015).
[39] P. G. Lagoudakis, P. G. Savvidis, J. J. Baumberg, D. M. Whittaker, P. R. Eastham, M. S. Skolnick, and J. S. Roberts, Phys. Rev. B **65**, 161310(R) (2002).
[40] D. N. Krizhanovskii, D. Sanvitto, I. A. Shelykh, M. M. Glazov, G. Malpuech, D. D. Solnyshkov, A. Kavokin, S. Ceccarelli, M. S. Skolnick, and J. S. Roberts, Phys. Rev. B **73**, 073303 (2006).
[41] S. Klembt, T. Harder, O. Egorov, K. Winkler, R. Ge, M. Bandres, M. Emmerling, L. Worschech, T. Liew, M. Segev *et al.*, Nature (London) **562**, 552 (2018).
[42] D. R. Gulevich, D. Yudin, I. V. Iorsh, and I. A. Shelykh, Phys. Rev. B **94**, 115437 (2016).
[43] D. N. Krizhanovskii, A. P. D. Love, D. Sanvitto, D. M. Whittaker, M. S. Skolnick, and J. S. Roberts, Phys. Rev. B **75**, 233307 (2007).
[44] T. A. Fisher, A. M. Afshar, M. S. Skolnick, D. M. Whittaker, and J. S. Roberts, Phys. Rev. B **53**, R10469 (1996).
[45] *Spin Physics in Semiconductors*, edited by M. I. Dyakonov, Springer Series in Solid-State Sciences (Springer, Berlin, 2017), Vol. 157.
[46] I. A. Shelykh, A. V. Kavokin, Y. G. Rubo, T. C. H. Liew, and G. Malpuech, Semicond. Sci. Technol. **25**, 013001 (2009).
[47] F. Tassone and Y. Yamamoto, Phys. Rev. B **59**, 10830 (1999).
[48] M. Sich, J. K. Chana, O. A. Egorov, H. Sigurdsson, I. A. Shelykh, D. V. Skryabin, P. M. Walker, E. Clarke, B. Royall, M. S. Skolnick, and D. N. Krizhanovskii, Phys. Rev. Lett. **120**, 167402 (2018).
[49] P. G. Savvidis, J. J. Baumberg, D. Porras, D. M. Whittaker, M. S. Skolnick, and J. S. Roberts, Phys. Rev. B **65**, 073309 (2002).
[50] A. I. Tartakovskii, V. D. Kulakovskii, D. N. Krizhanovskii, M. S. Skolnick, V. N. Astratov, A. Armitage, and J. S. Roberts, Phys. Rev. B **60**, R11293 (1999).
[51] L. Viña, T. C. Damen, J. E. Cunningham, J. Shah, and L. J. Sham, Superlatt. Microstruct. **12**, 379 (1992).
[52] D. N. Krizhanovskii, K. G. Lagoudakis, M. Wouters, B. Pietka, R. A. Bradley, K. Guda, D. M. Whittaker, M. S. Skolnick, B. Deveaud-Plédran, M. Richard, R. André, and L. S. Dang, Phys. Rev. B **80**, 045317 (2009).
[53] R. Houdré, C. Weisbuch, R. P. Stanley, U. Oesterle, and M. Ilegems, Phys. Rev. Lett. **85**, 2793 (2000).
[54] M. O. Borgh, J. Keeling, and N. G. Berloff, Phys. Rev. B **81**, 235302 (2010).
[55] I. A. Shelykh, D. D. Solnyshkov, G. Pavlovic, and G. Malpuech, Phys. Rev. B **78**, 041302(R) (2008).
[56] M. Sun, I. G. Savenko, S. Flach, and Y. G. Rubo, Phys. Rev. B **98**, 161204(R) (2018).